Surface Science 617 (2013) 183–191

Contents lists available at ScienceDirect

Surface Science

journal homepage: www.elsevier.com/locate/susc

Oxygen on an Fe monolayer on W(110): From chemisorption to oxidation ☆

K. Freindl [a,*], E. Partyka-Jankowska [b], W. Karaś [c], M. Zając [d,e], E. Madej [a], N. Spiridis [a], M. Ślęzak [c], T. Ślęzak [c], D. Wiśnios [c], J. Korecki [a,c]

[a] Jerzy Haber Institute of Catalysis and Surface Chemistry, Polish Academy of Sciences, ul. Niezapominajek 8, 30-239 Kraków, Poland
[b] Faculty of Physics, University of Vienna, Strudlhofgasse 4, A-1090 Vienna, Austria
[c] Faculty of Physics and Applied Computer Science, AGH University of Science and Technology, al. Mickiewicza 30, 30-059 Kraków, Poland
[d] European Synchrotron Radiation Facility, BP220, F-38043 Grenoble, France
[e] Synchrotron Radiation Center SOLARIS, Jagiellonian University, ul. Gronostajowa 7/P-1.6, 30-387 Kraków, Poland

ARTICLE INFO

Article history:
Received 15 May 2013
Accepted 8 July 2013
Available online 13 July 2013

Keywords:
Oxygen adsorption
Fe monolayer on W(110)
Conversion electron Mössbauer spectroscopy
Density functional calculations
Electronic structure
Hyperfine interactions

ABSTRACT

The adsorption of oxygen on a pseudomorphic iron monolayer deposited on a W(110) surface was studied experimentally and theoretically. Standard surface characterization methods, such as Auger electron spectroscopy and low energy electron diffraction, and specific nuclear methods, such as conversion electron Mössbauer spectroscopy (CEMS) and nuclear resonant scattering of synchrotron radiation, combined with theoretical calculations based on the density functional theory allowed us to determine the structure of the oxygen adsorbate and the electronic properties of iron atoms with different oxygen coordinations. The oxygen-(3×2) structure on the iron monolayer was recognized and was interpreted to be a state with oxygen chemisorbed on the non-reconstructed surface with modest electron transfer from iron to oxygen. A transition from chemisorbed oxygen to the onset of Fe-oxidation is revealed by distinct changes in the CEMS spectra.

© 2013 The Authors. Published by Elsevier B.V. All rights reserved.

1. Introduction

In the past, monolayer (ML) films of iron on W(110) were widely investigated as a model two-dimensional ferromagnet [1] in which the magnetic properties interplay with and stabilize an unusual, pseudomorphic structure that is stretched by 10% [2]. In real systems, the intrinsic magnetic properties are masked by the adsorption of residual gases [3]. In a typical ultra-high vacuum (UHV) environment, this adsorption also leads to distinct changes in the low-energy electron diffraction (LEED) patterns [4] after exposure to residual gases (RG) of approximately 1 Langmuir (L). Such an exposure accompanies typical measurements that take several hours at $1^{*}10^{-10}$ mbar, and it is obvious that this effect cannot be neglected in a discussion of magnetic and electronic properties. In the early stages of RG adsorption in a system consisting of alternating monolayer and double-layer stripes, Elmers et al. [3] attributed a regular (2×2) structure to the double-layer areas, whereas a less-ordered (2×2) structure was observed on the monolayer. A prolonged exposure to RG induces the appearance of a (3×2) structure [4] that coexists with the (2×2) structure. A similar RG effect, including layer-dependent reactivity, was reported in more detail for the analogous system of an Fe monolayer on Mo (110) and was attributed to the adsorption of CO, CO_2, H_2O and O_2, the main constituents of the RG atmosphere. The final conclusion by Murphy et al. [5] is that the ordered structures arise from oxygen that was dissociatively adsorbed from CO or CO_2.

A low-dimensional Fe crystal in a structure that is modified from the bulk structure also presents a very interesting system from the perspectives of adsorption and reactivity. In this context, it is surprising that systematic direct studies of oxygen on an Fe monolayer on W(110) are lacking. The only study of this system by Nahm and Gomer [6] showed that the adsorption of oxygen at 90 K resulted in a gradual diminution in the intensity of the p (1×1) spots and eventually led to complete disorder after a dose of 11 L. Upon heating at 600 K, a diffuse p (3×1) pattern emerged. However, these observations cannot be representative for typical growth and adsorption temperatures, which are usually at or above room temperature (RT).

To fill this gap, we undertook studies of the initial adsorption of oxygen on an Fe monolayer on W(110). It is interesting to compare our observations to those for the (110) surface of bulk iron. At room temperature, molecular oxygen on the Fe (110) surface is adsorbed dissociatively through molecular precursors [7–9]. For coverages less than 0.5 ML, two primary superstructures were experimentally observed. The best established superstructure is p (2×2) [9,10], which is commonly attributed to a coverage of 0.25 ML. Upon further exposure, more complex structures are reported. Their description is frequently oversimplified as a c (3×1) superstructure [7,8,11–16]; however, it is evident that the pattern is more complex [17] and involves a large

☆ This is an open-access article distributed under the terms of the Creative Commons Attribution-NonCommercial-No Derivative Works License, which permits non-commercial use, distribution, and reproduction in any medium, provided the original author and source are credited.

* Corresponding author. Tel.: +48 126395165; fax: +48 124251923.
E-mail address: ncfreind@cyf-kr.edu.pl (K. Freindl).

0039-6028/$ – see front matter © 2013 The Authors. Published by Elsevier B.V. All rights reserved.
http://dx.doi.org/10.1016/j.susc.2013.07.011

oblique unit cell. The oxygen coverage associated with this structure is somewhat controversial and is reported to be between 1/4 and 2/3 by different authors [7,8,11,12,17,18]. At still larger coverages, it is believed that the oxygen is incorporated in the subsurface layers, and this is considered to be the onset of oxidation [8].

Neither the LEED patterns [11,15,17,19] nor the rare STM images [10,13] of oxygen adsorbed on Fe (110) find comprehensive interpretation in terms of atomic adsorption geometry. Erley et al. [9] and Miyano et al. [18] suggest that oxygen atoms are initially adsorbed in the long bridge sites. A similar adsorption geometry was predicted theoretically by Blonski et al. [20]; however, very recent theoretical studies [21] by the same group showed that if a larger surface cell is considered in the calculation, the pseudo-threefold hollow sites become the most stable (see Fig. 1 for the definitions of the adsorption sites).

Compared to the Fe (110) surface of bulk iron, the pseudomorphic Fe monolayer on W(110) [psML-Fe/W(110)] presents a much more complex object. The properties of this monolayer should be influenced by the modified (increased) atomic distances and the proximity of the tungsten atoms, which are some first and all second neighbors. Through these influences, the studied systems may reflect some properties typical of nanostructures, such as those used in catalysts or sensors, especially bimetallic catalysts [22,23] in which enhanced and selective reactivity is induced by size effects and the synergy of the constituents.

The aim of this work is to describe the initial adsorption of oxygen on psML-Fe/W(110) from the perspective of the adsorption geometry and the chemical state of iron. To this end, we applied classical surface methods, i.e., low-energy electron diffraction (LEED) and Auger electron spectroscopy (AES), and nuclear methods, i.e., conversion electron Mössbauer spectroscopy (CEMS) and nuclear resonant scattering of synchrotron radiation (NRS). This combination of experimental methods ensures a complete characterization of the structural and electronic properties. For ultra thin iron films CEMS [24] and NRS [25] performed under UHV conditions are especially beneficial. The main advantage of these methods, which probe the hyperfine interactions, is the high sensitivity to the local symmetry and chemical state of the Fe atoms. For the present experiment performed at RT, only the electric interactions, a monopole resulting in the isomer shift (IS) and a quadrupole resulting in quadrupole splitting (QS), are of importance because the iron monolayer is in a paramagnetic state and there is no magnetic splitting of the hyperfine spectra (for basic information concerning hyperfine interactions as observed by Mössbauer spectroscopy refer to [26]). IS is proportional to the total electron density ρ^{tot} (0) at the nucleus (s-electrons); thus, IS characterizes the valence state of Fe. For iron, IS and ρ^{tot} (0) are negatively correlated. In the absence of magnetic interactions, the Mössbauer spectrum splits into two lines spaced by:

$$QS = \frac{eqV_{zz}}{2}\sqrt{1+\frac{\eta^2}{3}}, \quad (1)$$

where e is the electron charge, q is the nuclear quadrupole moment, V_{zz} is the main component of the diagonalized electric field gradient (EFG) tensor and η is the asymmetry parameter. If the asymmetry parameter is neglected, for the given values of the physical constants that determine the QS value, a simple relation can be drawn between QS and V_{zz} for ^{57}Fe: V_{zz} [10^{21} V/m^2] ≈ 1.5 QS [mm/s], where a 10% uncertainty of QS results from the experimental values of the nuclear quadrupole moment. QS reflects the asymmetry of the electronic charge distribution. Experimental [27] and theoretical [28] papers showed that the surface EFG sensitively probes the local symmetry and coordination and can be used for structural studies. A theoretical model is indispensable for a quantitative interpretation of the hyperfine interactions; therefore, our experimental study was complemented by calculations based on density functional theory (DFT). In this way, we were able to acquire deeper insight into the transient stage between oxygen adsorption and oxidation.

2. Details of the experiments and calculations

The experiments were performed in two different UHV systems dedicated to CEMS and NRS measurements. Both systems are equipped with molecular beam epitaxy facilities for the deposition of iron and for standard surface characterization methods: LEED and AES.

The W(110) substrate was cleaned through cycles of annealing at 1600 K under an oxygen pressure of 10^{-7} mbar, followed by flash heating at 2100 K under UHV conditions. The surface purity of the substrate was controlled by AES and LEED and occasionally by XPS as well. A perfect (1 × 1) pattern was recorded for the cleaned crystal. Iron was deposited from an effusion cell (BeO crucible) or with an electron beam evaporator. The deposition was monitored with a quartz crystal, which allowed us to estimate the coverage with an accuracy of 0.1 ML. Additionally, in the NRS system, the thickness could be calibrated directly through the in-situ X-ray reflectivity. For the pseudomorphic monolayer, we used a nominal coverage of 0.81 of the bulk Fe (110) monolayer, and this coverage corresponds to a monolayer thickness of 1.66 Å. To ensure continuity of the monolayer [29,30], an elevated deposition temperature (between 670 K and 770 K) was used. The typical deposition rate was 1 Å*min^{-1}. For CEMS and NRS, we used iron

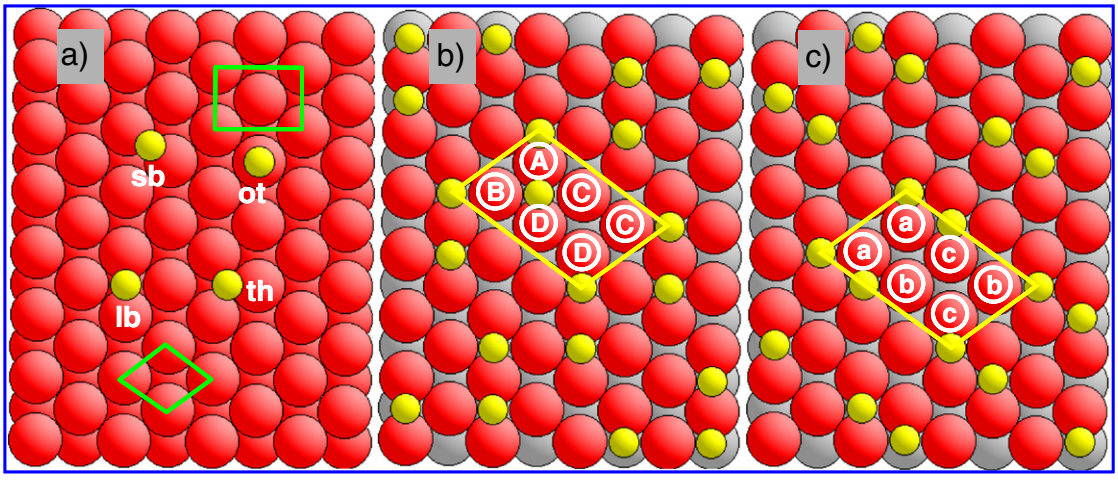

Fig. 1. a) The (110) surface of BCC iron. Indicated are: the primitive oblique (1 × 1) unit cell, the rectangular, centered, non-primitive (1 × 1) unit cell and the surface adsorption sites, including the long-bridge (lb), short-bridge (sb), pseudo-three fold hollow (th) and on top (ot) sites. b) and c) Two simple models of the O (3 × 2) adsorption structure on the Fe (110) monolayer on W(110) for oxygen adsorbed at the long bridge sites; in the text, these models are referred to as "Model-I" (b) and "Model-II" (c). The letters denote iron atoms with different oxygen coordination.

enriched with the ^{57}Fe isotope at 95%. Molecular oxygen with a purity of 5.0 N was dosed with a precise leak valve. Adsorption proceeded at RT at a partial pressure between 1×10^{-9} and 1×10^{-7} mbar.

To investigate the electronic properties, in addition to the standard surface methods of AES and XPS, we applied isotope-specific CEMS and NRS methods. In the CEMS system, the Mössbauer spectra were measured using a constant-acceleration spectrometer, as described previously [24]. The spectrometer used a large opening channeltron as a conversion electron detector, and a 100 mCi ^{57}Co (Rh) source that irradiated the sample under variable angle through a UHV beryllium window. Typically, the spectra were measured with gamma-rays along the surface normal ("N-geometry") and in a standard geometry ("S-geometry"), which ensured the optimum counting rate, at an incidence angle of 54° and at the azimuth along the [111] direction of the W(110) substrate. The average acquisition time for a ^{57}Fe-monolayer Mössbauer spectrum was several days.

The NRS experiment was performed at the nuclear resonance beamline ID18 [31] at the European Synchrotron Radiation Facility with a recently constructed UHV multichamber system [4,25]. The sample was illuminated in grazing incidence geometry under an angle of 5 mrad, which is the critical angle for the Fe/W system [32]. The direction of the synchrotron beam was parallel to the [110] direction in the W(110) surface, if the small grazing angle is neglected. The average acquisition time for a ^{57}Fe-monolayer NRS spectrum was approximately 1 h.

The measurement time is a crucial issue for reactive surfaces. In experiments with long durations, one must account for the adsorption of residual gases, which can significantly modify the properties of the surface. In this respect, NRS has an advantage over CEMS; however, the interpretation of the NRS time spectra is a much more complicated problem, and a certain ambiguity of the numerical analysis of the spectra can be overcome with a combination of both methods.

The experimental results were interpreted by a comparison with DFT calculations of the hyperfine parameters with the Wien2k software package [33] using the generalized gradient approximation and Perdew–Burke–Ernzerhof exchange–correlation functional [34]. The studied system of psML-Fe/W(110) was approximated by a slab of seven W(110) atomic layers with the pseudomorphic Fe monolayer on each side. A $3 \times 5 \times 1$ k-point mesh was used. The radii of the muffin-tin spheres were: 1.16 Å for tungsten, 1.0 Å for iron and 0.79 Å–0.85 Å for oxygen, depending on its distance from the surface. For the calculation of the Fermi energy a tetrahedron method was applied [35]. The entire system was relaxed, and this process led to an Fe–W interlayer spacing of 1.93 Å, which is in good agreement with previous data obtained with the VASP code [2]. For the adsorption of oxygen, a (3×2) unit cell was chosen, and the oxygen positions were only relaxed along the slab normal. The buckling and horizontal shifts of the atoms were neglected in the calculation. The energy and charge convergence criterions (the last more important for the hyperfine field calculations) were set to 10^{-3} eV and 10^{-3} electron, respectively.

3. Results

3.1. Adsorption structure

The LEED pattern of the as-deposited 1psML-Fe/W(110) presents a sharp (1×1) structure (Fig. 2a) with a diffuse background that is only slightly enhanced relative to the diffraction patterns of the background-free W(110) substrate. Upon the initial RT dosing with oxygen, which typically took place at 5×10^{-9} mbar, the onset of the (3×2) pattern was already apparent at an exposure of 0.2 L. This structure existed up to an exposure of 5–6 L and was most intense at approximately 4 L (Fig. 2b). The (3×2) structure that was previously observed for this system as a result of residual gas adsorption only [4] is discussed in detail below. With further exposure, the pattern became more complex; nevertheless, some typical superstructures could be distinguished, as shown in Fig. 2c–f. The modification of the (3×2) structures begins with the characteristic arcs that appear around the inner spots (Fig. 2c) and that gradually split into a new structure (Fig. 2d, exposure of 17 L), which combines the (5×1) structure, the (1×3) structure and some additional spots of an unidentified structure. At an exposure of approximately 70 L, the (5×1) structure dominates (Fig. 2e). Further stages of adsorption are characterized by the gradual simplification of the discrete pattern accompanied by an increase in the diffuse background. The ultimate structure, at an exposure of 150 L, is shown in Fig. 2f and is a combination of the (1×1) Fe/W(110) spots and a hexagonal pattern, which we attribute to an FeO oxide.

It should be noted that, if the Fe coverage exceeds 1psML, an additional (2×2) structure precedes the (3×2) structure. In agreement with Murphy et al. [5], this (2×2) structure must be associated with the second atomic layer and is clearly eliminated for a strict monolayer film of Fe.

The interpretation of the (3×2) LEED pattern is shown in Fig. 3a. The spots arise from two mirror domains resulting from the twofold symmetry. The corresponding periodicity in real space is shown in Fig. 3b. The primitive unit cell of the (3×2) superstructure [with respect to the primitive oblique unit cell of the (110) surface] is also oblique. However, a centered rectangular unit cell can also be introduced, and in the Wood notation, this rectangular superstructure is $\left(\sqrt{3}\times 2\sqrt{6}\right)R35$ with respect to the centered rectangular surface structure.

It is essential to associate the observed structures with the oxygen coverage. To do this, we exploited measurements of the oxygen Auger peak intensity (the KLL transition at 510 eV) as a function of the oxygen exposure. The resulting uptake curve in a broad exposition range is presented in Fig. 4a, and the inset shows a low exposure range in more detail. The initial slope of the uptake curve indicates a high sticking coefficient, than there is a plateau between 1 and 4 L, which corresponds to the (3×2) structure. It should be noted that the preparation for the first Auger measurement already induces some contamination of the surface, and a small oxygen signal is visible prior to the O_2 adsorption. At further exposure the uptake curve saturates rather quickly, and at an exposure of 50 L, the observed oxygen signal is 90% of the saturation signal. Under the assumption that this saturation value corresponds to one oxygen monolayer, the coverage corresponding to the (3×2) structure is estimated to be approximately 1/3. Within the observed unit cell, which is six times larger than the iron surface cell, we conclude that one third of the adsorption sites are occupied by oxygen. Obviously, such a coverage, combined with the symmetry observed by LEED, can be realized by many different atomic configurations, which also depend on the preferences for adsorption sites. The two simplest examples of the oxygen adsorption geometry for the (3×2) structure with oxygen adsorbed at the long bridge sites are shown in Fig. 1. Other, more complex adsorption structures may include alternative adsorption sites (e. g., the pseudo-three fold hollow) and/or buckling in both the iron and oxygen layers.

The adsorption process was also monitored by the changes in the MVV Fe Auger signal at approximately 45 eV, as shown in Fig. 4b. Upon the initial adsorption, including the exposure range corresponding to the (3×2) structure, the only effect of the oxygen is a reduction in the iron intensity; this single effect means that this chemisorption stage does not induce any severe modification of the Fe valence band structure. At higher oxygen coverages, i.e., 20 L and greater, the shape of the MVV Fe lines changes considerably by displaying some features that are also observed for oxidized 1MLFe/Cu (100) [36]. Independent of the complex character of the changes in the Fe MVV peak shape [36–38], it is obvious that oxygen has only a limited impact on the electronic structure of iron in the chemisorbed state that corresponds to the (3×2) structure. We understand that in this state the oxygen is bonded to the Fe layer at the adsorption sites characteristic of a BCC (110) surface. The appearance of the more complex structures above the (3×2) structure, as documented in LEED, indicates the beginning

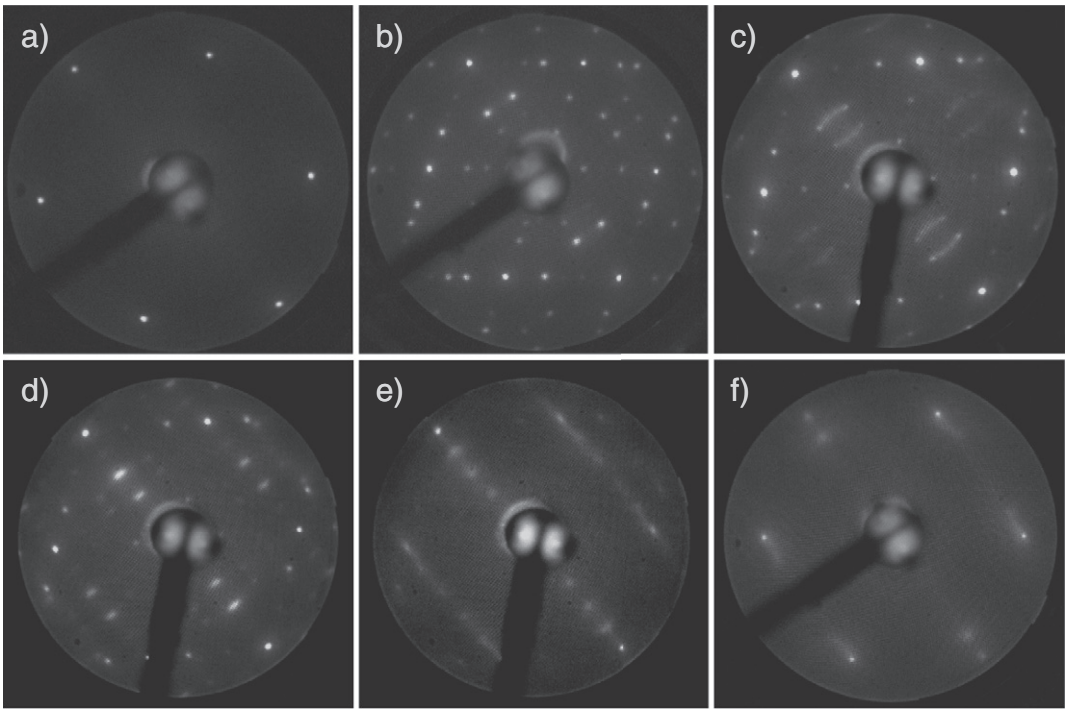

Fig. 2. LEED patterns at an electron energy of 55 eV for psML-Fe/W(110) as-prepared (a) and after the adsorption of oxygen at room temperature at exposures of 2.2 L (b), 10 L (c), 17 L (d), 72 L (e) and 152 L (f).

of oxidation, which we understand to be the formation of Fe–O bonds that modify the local Fe coordination and require a rearrangement of the positions of the iron atoms. Returning to the corresponding LEED patterns, one can correlate the first phase of oxidation with the (5×1) LEED structure. Then, this (5×1) structure is a coincidence structure between the hexagonal lattice of FeO with an in-plane distance of 3.04 Å [9] and the centered rectangular lattice of psML-Fe/W(110). The surface rectangular lattice perfectly fits the FeO spacing along the [100] direction, whereas a 20% misfit is present along the $[1\bar{1}0]$ direction. Further adsorption establishes the hexagonal LEED pattern that corresponds to the FeO-phase. A change of the chemical structure is also seen in the Auger spectra. Such a strong interaction is reflected in the modification of the electronic structure of iron and can be distinctly observed by surface spectroscopic methods [39].

For the most stable (3×2) structure, which is the central point of this paper, the changes in the electronic structure of iron induced by the chemisorbed oxygen were faint and were barely accessible by Auger or core excitation XPS (spectra not shown). However, these changes contributed to measurable changes in the hyperfine interactions, which are sensitive to local coordination and to small changes in the valence electron densities, as shown in the next section.

3.2. CEMS and NRS data

The chemical state of the iron atoms interacting with oxygen that forms the stable O-(3×2) structure on psML-Fe/W (110) were probed with NRS and CEMS. The analysis of the iron hyperfine pattern corresponding to this structure is based on the understanding of the clean

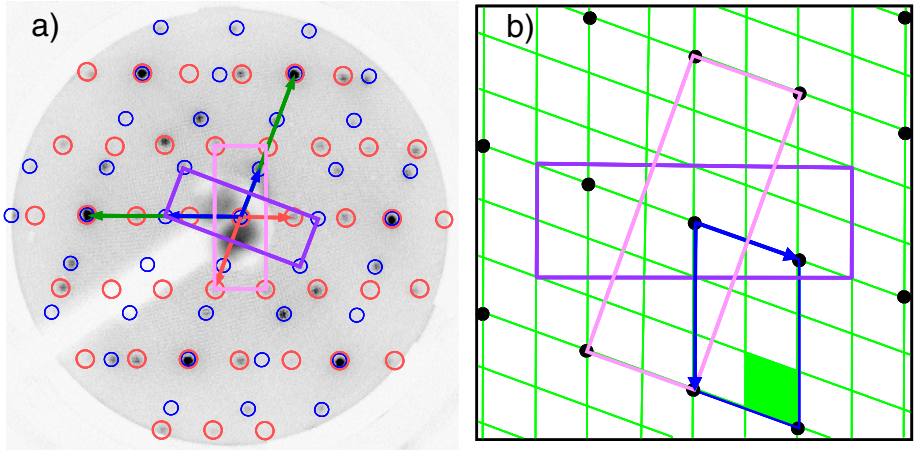

Fig. 3. a) Interpretation of the LEED pattern for the O (3×2)/psML-Fe/W(110) superstructure. Spots from two rotational domains are shown by circles of different colors (and sizes). The basis vectors for the reciprocal lattice of the substrate (green), for the adsorbate structure (blue/red) and for the unit cells of the reciprocal centered rectangular lattices are shown. b) The real space sketch of the O (3×2)/psML-Fe/W(110) superstructure lattice marked by black points on the substrate mesh. The basis (3×2) vectors of the real oblique superstructure lattice and the center rectangular unit cells of the two rotational superlattice domains are shown.

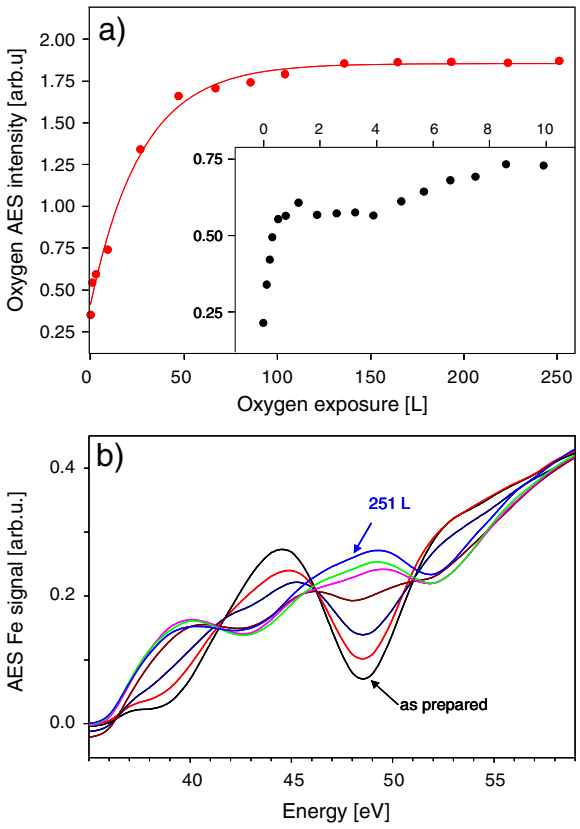

Fig. 4. a) The amplitude of the oxygen Auger line is shown as a function of the exposure of psML-Fe/W(110) to oxygen. The inset shows a low exposure range (0–11 L) in more detail. b) The change in the AES Fe MVV signal with increasing oxygen exposure at 0 L (the as-prepared monolayer), 1 L, 9 L, 27 L, 47 L, 67 L and 251 L.

psML-Fe/W (110) spectra that are shown in Fig. 5. The NRS spectrum for the pristine as-prepared state (Fig. 5a) reveals a simple exponential decay, as discussed in our previous paper [4]. Such a beat-less spectrum corresponds to a special case, in which the main axis of the electric field gradient (EFG) is perpendicular to the polarization vector and to the wave vector of the incoming synchrotron radiation. For the given experimental geometry (grazing incidence), this spectrum occurs when the main EFG axis is along the surface normal. Under these conditions, the strength of the EFG is not accessible; however, this information can be determined from the complementary CEMS measurements, notwithstanding the influence of residual gas adsorption, which is unavoidable for the long-duration Mössbauer experiment. Whereas the NRS time spectra are very sensitive to the EFG orientation, the CEMS spectra directly reveal the magnitude of the electric field gradient by the quadrupole splitting, as demonstrated by the spectrum shown in Fig. 5b. The spectrum is dominated by an asymmetric doublet with the hyperfine parameters, the quadrupole splitting and isomer shift equal to QS = 0.72(3) mm/s and IS = 0.24(2) mm/s, respectively. Because of the long acquisition time (48 h), these parameters can differ slightly from those of the pristine monolayer; this difference is in agreement with the change in the LEED pattern before and after measurement, which clearly shows the influence of the RG adsorption [4]. However, the time evolution of the spectra (partial spectra were also recorded) does not indicate strong changes in the QS and IS values with measurement time. From the fit of the partial spectra, a tendency for a slight increase in QS is observed with the RG adsorption; this tendency is in agreement with previous NRS studies [4]. The asymmetry of the doublet lines indicates that a preferred direction of the main EFG component exists [41]. The intensity ratio (A_1/A_2) of the doublet lines is determined by the orientation of the principal EFG axis (Z) according to the formula: $A_1/A_2 = \frac{1+\cos^2\theta}{5/3-\cos^2\theta}$, where θ is the angle between the propagation of the γ-rays and the Z-axis and the relative position of the doublet lines numbered "1" or "2" at the velocity scale depends on the sign of the EFG. In agreement with NRS, the average direction of the principal EFG axis for the Fe-monolayer affected by RG is tilted from the normal by approximately 30°.

The starting point for the analysis of the hyperfine interactions for the psML-Fe/W(110) with the (3 × 2) oxygen structure are the CEMS spectra, which are measured in different geometries, as shown in Fig. 6. It must be noted that, contrary to the measurements for a pristine Fe monolayer, the LEED patterns before and after long-standing CEMS experiments were practically unchanged. This observation, which is important from a methodological point of view, also indicates that the (3 × 2) structures are highly stable under exposure to RG (mainly hydrogen) on the order of 50 L.

The adsorption models proposed in Fig. 1 give some indications concerning the fitting of the CEMS spectra; in particular, these models suggest a minimum number of different spectral components (Fe-sites). Formally, the unit cell of the (3 × 2) structures contains four or three distinct types of Fe atoms in "Model-I" and "Model-II", respectively. For a preliminary interpretation of the spectra, "Model-I" was considered because the corresponding sites (denoted by A, B, C and D in Fig. 1b) can be grouped into two types based on features, such as number of oxygen neighbors or distance and direction of oxygen neighbors, that can influence the electron transfer between iron and oxygen. Consequently, one can expect (i) similarity between the A and B sites and the C and D sites if the number of oxygen atoms is decisive or (ii) similarity between the A and D sites and the B and C sites if the distance and direction are decisive. These two cases result in different weights for the spectral components of 1:2 or 1:1, respectively. Such an initial simplified analysis, with two spectral components only, was performed according to (i) and (ii), and in this analysis, a distribution of the hyperfine parameters was considered using a suitable fitting procedure. The spectra

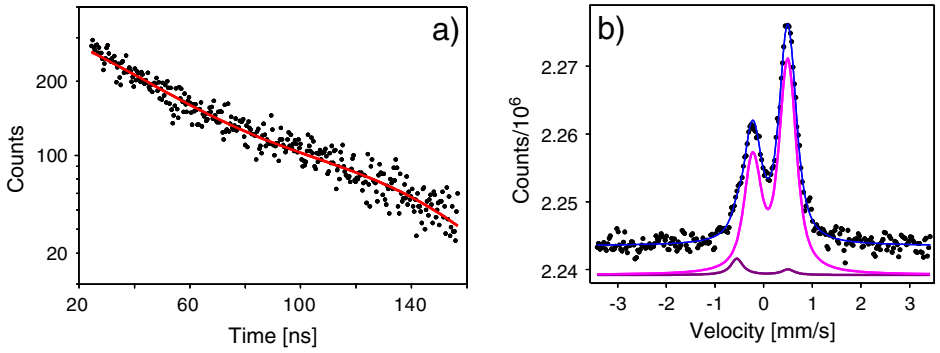

Fig. 5. a) NRS spectrum of the clean psML-Fe/W(110). The dots represent the experimental data, the solid line is the best fit obtained with the CONUSS software [40]. b) CEMS spectrum of the nominally clean psML-Fe/W(110). The fitted spectral components (two quadrupole doublets) are offset in the y-axis for clarity.

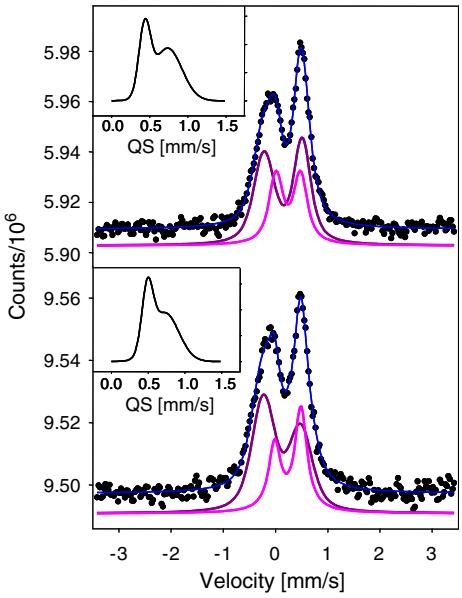

Fig. 6. CEMS spectra of psML Fe/W(110) with the (3 × 2) oxygen structure for two measurement geometries. The γ ray perpendicular to the sample surface is the "N-geometry" (top), and the γ ray at 54° to the normal is the "S-geometry" (bottom). The fitted spectral components (for simplification, only two quadrupole sites were used) are offset in the y-axis for clarity. The insets show the QS distributions.

were fitted using the Recoil software [42] by a convolution of quadrupole doublets composed of Lorentzian lines with a Gaussian distribution of the quadrupole splittings. Additionally, the isomer shifts and the quadrupole splittings were assumed to be linearly correlated. Within the above simplifications, both assumptions (i) and (ii) gave reasonable results; case (i) is shown as an example by the solid lines in Fig. 6, and the corresponding QS distributions are shown in the insets in Fig. 6 and are summarized in Table 1. Both fits reveal similar IS and QS values for the corresponding spectral components. One component is similar to the dominant component of the clean monolayer and indicates that the influence of oxygen does not extent much beyond a small electron transfer and does not result in the formation of well-defined ionic states of Fe.

In the standard measurement geometry, both fits differ remarkably in the intensity ratio of the doublet lines, and this difference reflects the sensitivity of the spectra to the geometry of the adsorption. Because the sign of the EFG is a priori unknown in the fits, A_1 and A_2 correspond to the line with the more negative and more positive velocity, respectively. Additionally, if the Z-axis is tilted from the surface normal, a similar intensity ratio corresponds to a different EFG orientation, especially if the azimuthal direction of Z-axis differs for different sites. For these reasons, the determination of the EFG orientation from the CEMS spectra becomes ambiguous. To fully take advantage of the strong CEMS sensitivity to the chemical state, comparison with theory is necessary to interpret the IS and QS values.

3.3. Comparison with theory

The interpretation of the experimental results was based on Wien2k calculations of the hyperfine parameters. The theoretical methodology was crosschecked by calculating the hyperfine parameters at the Fe (110) surface, which was approximated as a slab of seven Fe (110) atomic layers and for which experimental data are available in the literature [43,44]. The present calculations of the surface hyperfine magnetic field and isomer shift agree well with the theoretical data by Fu and Freeman [45], nicely fit the experimental data for the surface electric field gradient and explain the orientation of the principal EFG axis at the Fe (110) surface, which is along the surface normal, as was intuitively assumed in the experimental paper [43]. The clean Fe (110) surface values for the calculated electrical gradient and isomer shift are $V_{zz} = 4.08{*}10^{21}$ V/m^2 and IS = 0.04 mm/s, where the proportionality constant $\alpha = 0.291$ in the relation $IS = -\alpha \cdot [\rho^{tot}(0) - \rho^{tot}_{ref}(0)]$ was taken from Ref. [46], and the reference electron density, $\rho^{tot}_{ref}(0)$, which in experiments usually refers to metallic iron, is taken in the present calculation as the value for the center of the seven layer Fe (110) slab. Methodologically, it is important to note that the approximation of the bulk surface with a slab geometry introduces some systematic shifts in V_{zz} and IS due to the lack of translational symmetry; thus, only relative differences between the surface and central slab layers are meaningful. This approximation causes certain ambiguity in calculations for psML-Fe/W(110) because there is no direct reference to the central Fe layers for this system.

The results of the calculations for clean psML-Fe/W(110) and two model adsorption structures are presented in Table 2. The resulting electronic structure for the clean iron monolayer can be compared with calculations by Łażewski et al. [2]; these calculations were performed with a different code for a similar system based on a three-layer tungsten slab. The spin-resolved density of states (DOS) shown in Fig. 7 (top) reproduces all of the important features noted by Łażewski et al., such as the downward shift of the majority band, the narrowing of the majority band (relative to the bulk) and the corresponding changes in the minority band. This band structure results in a slightly increased value in the magnetic moment of the ground state ($\mu_{mono} = 2.42\ \mu_B$, $\mu_{bulk} = 2.25\ \mu_B$ for the monolayer and for the center of the seven layer slab, respectively). Remarkably, although the states at the Fermi level for the bulk are dominated by the majority spins, in the monolayer, the minority spins clearly prevail.

The monolayer IS only differs slightly from that of bulk Fe and shifts towards positive value (IS = +0.06, relative to the central layer of the seven layer Fe (110) slab); however, this value must be treated with some reservations because of an ambiguity in the reference IS. The EFG value reflects the distribution of the charge density around the probe atom. The principal axis of the EFG is perpendicular to the surface, and the V_{zz} component is positive. Additionally, the hyperfine magnetic field $B_{hf} = 12.8$ T (which is inaccessible in the present experiment because of the low Curie temperature) is very different from the bulk value (34 T) because of the partial compensation between the contributions from the local and the transferred hyperfine magnetic fields [47],

Table 1
Hyperfine parameters derived from the CEMS spectra for the O (3 × 2) structure fitted with two doublet components with spectral weights of 1:2 and 1:1. QS is the quadrupole splitting, ΔQS is the Gaussian width of the QS distribution, IS is the isomer shift relative to α-Fe, and A_1/A_2 is the intensity ratio of the doublet lines.

Measurement geometry	Constraints of the fit	Spectral component	QS [mm/s]	ΔQS [mm/s]	IS [mm/s]	A_1/A_2	Spectral weight
Perpendicular -"N"	Doublet intensity 1:2	Doublet 1	0.43	0.08	0.34	1	1
		Doublet 2	0.74	0.19	0.25	1	2
	Doublet intensity 1:1	Doublet 1	0.55	0.03	0.36	1	1
		Doublet 2	0.72	0.02	0.22	1.1	1
Standard -"S"	Doublet intensity 1:2	Doublet 1	0.46	0	0.34	0.9	1
		Doublet 2	0.73	0.13	0.24	1.17	2
	Doublet intensity 1:1	Doublet 1	0.46	0.1	0.34	0.46	1
		Doublet 2	0.73	0.14	0.25	3	1

Table 2
Results of the DFT calculations: hyperfine parameters of the Fe (110) monolayer with and without adsorbed oxygen. IS is the isomer shift relative to the value derived for the central layer of a 7-layer Fe slab, V_{zz} is the calculated value of the main component of the electric field gradient (EFG), the V_{zz} orientation column gives the angle between the principal axis of the EFG (z-axis) and the sample normal, QS is the quadrupole splitting calculated according to formula (1), and B_{hf} and μ are the hyperfine magnetic field and the magnetic moment, respectively, calculated for a ferromagnetic state.

		Fe site	IS[mm/s]	QS[mm/s]	$V_{zz} \cdot 10^{21}$ [V/m^2]	V_{zz} orientation	B_{hf}[T]	μ [μ_B]
1 × 1	Clean monolayer		0.06	1.06	5.00	0°	12.8	2.42
3 × 2	O (3 × 2) "Model-I"	A	0.08	0.83	3.60	90°	11.5	2.42
	(Fig. 1 b)	B	0.27	−0.99	−4.74	90°	19.1	2.41
		C	0.18	0.91	3.87	10°	17.7	2.46
		D	0.07	−1.24	−5.25	119°	14.8	2.42
	O (3 × 2) "Model-II"	a	0.12	−1.31	−6.14	117°	13.6	2.46
	(Fig. 1 c)	b	0.06	−1.21	−5.45	121°	13.8	2.46
		c	0.17	0.85	3.69	2°	17.6	2.48

and this value agrees fairly well with the experimental value measured for a similar system [48].

The adsorption calculation was performed for the two simple geometrical models introduced in the previous section. For both models, the local Fe-DOS for the given sites are shown in Fig. 7 (center and bottom). In accordance with the intuition that a more homogenous distribution of oxygen atoms is energetically more stable, "Model-I" gave the total energy lower by 2.5 eV. Generally, the adsorption of oxygen induces broadening of the band and substantially lowers the spin polarization at the Fermi level. Additionally, different atoms in both the models show different hybridization with oxygen, as observed in both the bottom of the majority band and the top of the minority Fe-bands through comparison with the oxygen DOS (not shown). In particular, in "Model-II", for atoms *a* and *c*, a distinct state appears at an energy of approximately −5.5 eV; this state arises from the hybridization between the O 2p orbitals and Fe valence orbitals. This state contributes to the Fe–O bonding. Remarkably, no such bond formation is observed for the *b* atom. The DOS is even more diverse in "Model-I", in which the *A* atom shows the strongest influence from oxygen (the highest peak at −5.5 eV and the flattening of the majority d-band), whereas the *D* atom shows only few signs and the *B* and *C* atoms show no signs of bond formation with oxygen. Through an analysis of the coordination of the Fe atoms in the discussed models, it becomes clear that the strongest Fe–O bond is formed for the oxygen atoms that are the closest to Fe and is independent of the number of oxygen neighbors.

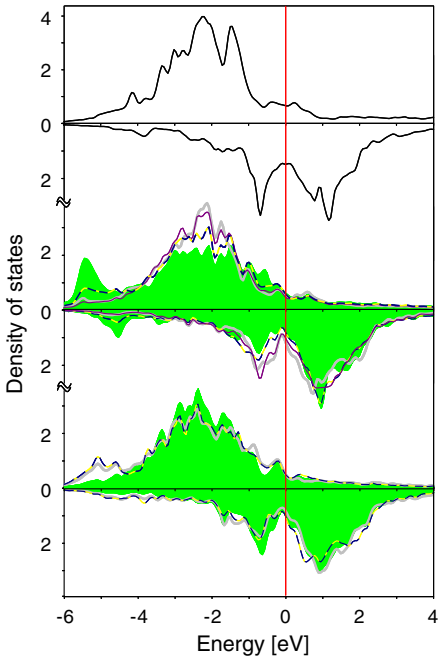

Fig. 7. Calculated spin-resolved, Fe valence electron density of states for the clean psML-Fe/W(110) (top) and for the O-(3 × 2) structure for "Model-I" (center) and "Model-II" (bottom). Iron atoms with different oxygen coordination are denoted with different line styles or shadings of the curve. For "Model-I": atom A–shaded, atom B–light solid line, atom C–dark solid line, atom D–dashed line; for "Model II": atom a–dashed line, atom b–light solid line, atom c–shaded. The spin-up states are in the positive direction of the y axis; the spin-down states are in the negative direction of the y axis.

In view of the present calculations, it becomes understandable that Nahm and Gomer [6] observed a metallic-like Fe 2p photoemission spectrum for oxygen chemisorbed on psML-Fe/W(110). Practically, only spin-polarized photoemission spectroscopy, which probes the spin-polarization at the Fermi level, would be capable of reflecting the subtle changes in the electronic structure induced by the chemisorbed oxygen. In the following, we show that the Mössbauer parameters sensitively probe the chemisorption of oxygen.

Relatively small changes in the electronic structure are accompanied by distinct modification of the hyperfine parameters caused by oxygen adsorption. These modifications are characterized by a systematic increase in the isomer shift for certain Fe sites, variation in the principal component of the EFG and, more importantly, by significant changes in the point charge symmetry, which are reflected in the sign and direction of the principal EFG component. These features should be strongly reflected in the Mössbauer spectra in the intensity of the doublet lines and give a sensitive criterion for verification of the different adsorption models.

The applicability of the model was tested by simulating the CEMS spectra using spectral components that exactly corresponded to the theoretical values from Table 2. Obviously, "Model-II", which results in three different spectral components corresponding to sites a, b and c, and equally weighted, does not reflect the character of the experimental spectrum, as shown in the inset to Fig. 8. On the contrary, for "Model-I", despite some systematic discrepancies in the experimental and simulated spectra, the shape of the spectrum is well reproduced by the model data. The consistency between theory and experiment could easily be improved by allowing homogenous linear scaling of the hyperfine parameters, IS and QS; this scaling is acceptable because of the ambiguity in the proportionality constants between the electronic properties and the hyperfine data [49]. A final improvement in the agreement between the experiment and theory is achieved with fits of the spectra that include a small (approximately 10%) variation in the IS, QS, doublet intensity ratio and contribution of a given spectral component. The resulting fits according to "Model-I" are fully consistent for both measurement geometries, as shown by the fitted spectra in Fig. 8. The structure described by "Model-I" is also more stable from the total energy point of view.

4. Conclusions: from chemisorption to oxidation

The Mössbauer spectra of psML-Fe/W(110) with the O (3 × 2) superstructure allowed us to identify the different adsorption sites and the accompanying chemical states of the iron atoms with different

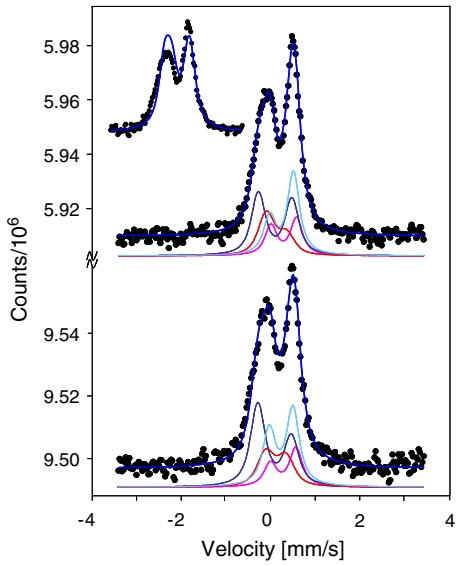

Fig. 8. CEMS spectra of psML-Fe/W(110) with the O (3 × 2) adsorbate structure measured in two geometries. The γ ray perpendicular to the sample surface is the "N-geometry" (top), and the γ ray at 54° to the normal is the "S-geometry" (bottom). The fits are based on the hyperfine parameters calculated for "Model-I" of the adsorbate geometry structure. The inset shows the simulation of the perpendicular spectrum based on the parameters from "Model-II," which clearly does not fit the experimental spectrum.

electronic structures. The observed spectral features (i.e., the parameters of the hyperfine interactions) could be interpreted using a simple adsorption model in which the (3 × 2) surface unit cell is occupied by two oxygen atoms that form zigzag rows in the [111] direction. Although the calculated DOS's show the onset of the formation of Fe – O bonds, the isomer shift values indicate modest electron transfer from the iron to oxygen rather than the existence of iron cations with well-identified valency states.

The chemisorption state identified for the (3 × 2) structure following the low oxygen doses (approximately a dozen Langmuirs) precedes the oxidation phase, which is observed in the Auger spectra and in the LEED pattern through new maxima and a change of symmetry, respectively. The transition from chemisorption to oxidation proceeds through the (5 × 1) structure, which further develops into the hexagonal pattern characteristic for the (111) face of FeO oxide, as shown in Fig. 2f. The corresponding Mössbauer spectrum is shown in Fig. 9.

The spectrum is very different from that of the chemisorbed state through large positive isomer shifts and through a component with remarkably enhanced quadrupole splitting. Such a spectrum represents the typical features observed for oxides in a divalent state and

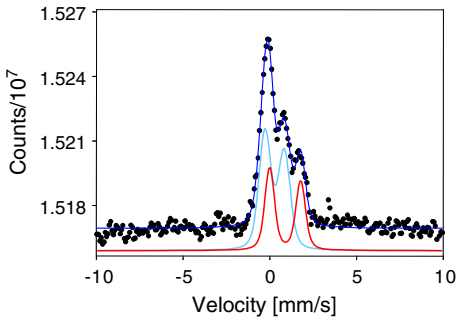

Fig. 9. CEMS spectrum of the strongly oxidized (oxygen exposure of 280 L) psML-Fe/W(110).

low local symmetry and can be easily explained by the low symmetry of the two-dimensional system. The two components observed in the spectrum can be explained either through a two-layer model with different layer-specific hyperfine parameters (one monolayer of Fe produces more than one monolayer of FeO) or through a structural model in which the iron atoms occupy two different positions, which result from reconstruction (buckling or horizontal shifts) of the FeO layer.

Acknowledgments

This work was supported in part by the National Science Center (NCN), Poland (Grant No. 2011/02/A/ST3/00150), by the Team Program of the Foundation for Polish Science cofinanced by the EU European Regional Development Fund, by the Polish-Austrian Scientific and Technological Cooperation Program, and by the Austrian Science Fund FWF project No. P-20713-N20. This research has received also funding from the Marian Smoluchowski Krakow Research Consortium–a Leading National Research Centre KNOW supported by the Ministry of Science and Higher Education. The calculations were performed in the ACK Cyfronet AGH, computational Grant No. NiSW/IBM_BC_HS21/AGH/035/2007.

References

[1] H.-J. Elmers, Int. J. Mod. Phys. B 9 (1995) 31115.
[2] J. Łażewski, P. Piekarz, A.M. Oleś, J. Korecki, K. Parliński, Phys. Rev. B 76 (2007) 205427.
[3] H.J. Elmers, J. Hauschild, U. Gradmann, Phys. Rev. B 59 (1999) 3688.
[4] E. Partyka-Jankowska, B. Sepiol, M. Sladecek, D. Kmiec, J. Korecki, T. Slezak, M. Zajac, S. Stankov, R. Rüffer, G. Vogl, Surf. Sci. 602 (2008) 1453.
[5] S. Murphy, G. Mariotto, N. Berdunov, I.V. Shvets, Phys. Rev. B 68 (2003) 165419.
[6] T.-U. Nahm, R. Gomer, Surf. Sci. 373 (1997) 237.
[7] G. Pirug, G. Broden, H.P. Bonzel, Surf. Sci. 94 (1980) 323.
[8] A. Hodgson, A. Wight, G. Worthy, Surf. Sci. 319 (1994) 119.
[9] W. Erley, H. Ibach, Solid State Commun. 37 (1981) 937.
[10] J. Weissenrieder, M. Göthelid, M. Månsson, H. Von Schenck, O. Tjernberg, U.O. Karlsson, Surf. Sci. 527 (2003) 163.
[11] J. Pignocco, G.E. Pellisser, Surf. Sci. 7 (1967) 261.
[12] Y. Sakisaka, T. Komeda, T. Miyano, M. Onchi, S. Masuda, Y. Harada, K. Yagi, H. Kato, Surf. Sci. 164 (1985) 220.
[13] A. Wight, N.G. London, F.M. Leibsle, G. Worthy, A. Hodgson, Surf. Sci. 331–333 (1995) 133.
[14] E. Vescovo, C. Carbone, W. Eberhardt, O. Rader, T. Kachel, W. Gudat, Surf. Sci. 48 (1993) 285.
[15] H.-J. Kim, E. Vescovo, Phys. Rev. B 58 (1998) 14047.
[16] M. Getzlaff, J. Bansmann, G. Schonhense, J. Magn. Magn. Mater. 192 (1999) 458.
[17] K. Molière, F. Portele, in: G.A. Somorjai (Ed.), The Structure and Chemistry of Solid Surfaces, Wiley, New York, 1968, p. 69-1.
[18] T. Miyano, Y. Sakisaka, T. Komeda, M. Onchi, Surf. Sci. 169 (1986) 197.
[19] M. Busch, M. Gruyters, H. Winter, Surf. Sci. 600 (2006) 4598.
[20] P. Blonski, A. Kiejna, J. Hafner, Surf. Sci. 590 (2005) 88.
[21] P. Blonski, A. Kiejna, J. Hafner, Phys. Rev. B 77 (2008) 155424.
[22] J.J. Kolodziej, T.E. Madey, J.W. Keister, J.E. Rowe, Phys. Rev. B 62 (2000) 5150.
[23] Z. Wang, F. Yang, S. Axnanda, C. Liu, D. Wayne Goodman, Appl. Catal., A 391 (2011) 342.
[24] N. Spiridis, D. Wilgocka-Ślęzak, K. Freindl, B. Figarska, T. Giela, E. Młyńczak, B. Strzelczyk, M. Zając, J. Korecki, Phys. Rev. B 85 (2012) 075436.
[25] S. Stankov, R. Rüffer, M. Sladecek, M. Rennhofer, B. Sepiol, G. Vogl, N. Spiridis, T. Ślęzak, J. Korecki, Rev. Sci. Instrum. 79 (2008) 045108.
[26] N.N. Greenwood, T.C. Gibb, Mössbauer spectroscopy, Chapman and Hall Ltd., London, 1972.
[27] T. Klas, J. Voigt, W. Keppner, R. Wesche, G. Schatz, Phys. Rev. Lett. 57 (1986) 1068; W. Körner, W. Keppner, B. Lehndorff-Junges, G. Schatz, Phys. Rev. Lett. 49 (1982) 1735.
[28] B. Lindgren, Z. Naturforsch. 57 a (2002) 544.
[29] H.J. Elmers, J. Hauschild, H. Höche, U. Gradmann, H. Bethge, D. Heuer, U. Köhler, Phys. Rev. Lett. 73 (1994) 898.
[30] H. Bethge, D. Heter, Ch. Jensen, K. Reshöft, U. Köhler, Surf. Sci. 331–333 (1995) 878.
[31] R. Rüffer, A.I. Chumakov, Hyperfine Interact. 97 (1996) 589.
[32] R. Röhlsberger, J. Bansmann, V. Senz, K.L. Jonas, A. Bettac, K.H. Meiwes-Broer, O. Leupold, Phys. Rev. B 67 (2003) 245412.
[33] P. Blaha, K. Schwarz, G.K.H. Madsen, D. Kvasnicka, J. Luitz, WIEN2K, An Augmented Plane Wave and Local Orbitals Program for Calculating Crystal Properties, Vienna University of Technology, Vienna, 2001.
[34] P. Perdew, K. Burke, M. Ernzerhof, Phys. Rev. Lett. 77 (1996) 3865.
[35] P.E. Blöchl, O. Jepsen, O.K. Andersen Phys, Rev. B 49 (1994) 16223.
[36] H. den Daas, O.L.J. Gijzeman, J.W. Geus, Surf. Sci. 209 (1993) 26.
[37] M. Seo, J.B. Lumsden, R.W. Staehle, Surf. Sci. 50 (1975) 541.

[38] V.S. Smentkowski, J.T. Yates Jr., Surf. Sci. 232 (1990) 113.
[39] Y. Joseph, G. Ketteler, C. Kuhrs, W. Ranke, W. Weiss, R. Schlögl, Phys. Chem. Chem. Phys. 3 (2001) 4141.
[40] W. Sturhahn, Hyperfine Interact. 125 (2000) 149.
[41] B. Roldan Cuenya, A. Naitabdi, E. Schuster, R. Peters, M. Doi, W. Keune, Phys. Rev. B 76 (2007) 094403.
[42] Ken Lagarec, 2002.
[43] J. Korecki, U. Gradmann, Phys. Rev. Lett. 55 (1985) 2491.
[44] T. Ślęzak, J. Łażewski, S. Stankov, K. Parliński, R. Reitinger, M. Rennhofer, R. Rüffer, B. Sepiol, M. Ślęzak, N. Spiridis, M. Zając, A.I. Chumakov, J. Korecki, Phys. Rev. Lett. 99 (2007) 066103.
[45] C.L. Fu, A.J. Freeman, J. Magn. Magn. Mater. 69 (1987) L1.
[46] U. Wdowik, K. Ruebenbauer, Phys. Rev. B 76 (2007) 155118.
[47] S.C. Hong, A.J. Freeman, C.L. Fu, Phys. Rev. B 38 (1988) 12156.
[48] M. Przybylski, U. Gradmann, Phys. Rev. Lett. 59 (1987) 1152.
[49] P. Blaha, J. Phys. Conf. Ser. 217 (2010) 012009.